Speckle masking in astronomy: triple correlation theory and applications

Adolf W. Lohmann, Gerd Weigelt, and Bernhard Wirnitzer

Due to the turbulent atmosphere the resolution of conventional astrophotography is limited to ~1 sec of arc. However, the speckle-masking method can yield diffraction-limited resolution, i.e., 0.03 sec of arc with a 3.6-m telescope. Speckle masking yields true images of general astronomical objects. No point source is required in the isoplanatic field of the object. We present the theory of speckle masking; it makes use of triple correlations and their Fourier counterparts, the bispectra. We show algorithms for the recovery of the object from genuine astronomical bispectra data.

I. Introduction

The resolution of conventional astrophotography with large telescopes is not limited by the diffraction on the finite aperture. The influence of the turbulent atmosphere is worse than aperture diffraction. Typically, the size of a turbulence bubble is 10 cm. Diffraction on these bubbles causes an angular blur of λ/d = 500 nm/10 cm ≈ 1 sec of arc). Therefore the resolution of conventional astrophotography is of the order of 1 sec of arc, which is much lower than the diffraction-limited resolution of large telescopes. For example, the diffraction-limited resolution of a 3.6-m telescope is 0.03 sec of arc for λ = 500 nm. This high angular resolution can be achieved by various interferometric methods[1-20] in spite of image degradation by the atmosphere. One of these methods is the speckle-masking method[8] which has recently been applied to astronomical data.[20] The raw data for speckle masking and also for most of the other speckle methods are speckle interferograms. Speckle interferograms are short-exposure photographs recorded in the image plane of large telescopes. The exposure time has to be shorter than ~0.1 sec in order to freeze the atmosphere. In this case the short-exposure photographs consist of an interferometric fine structure called speckles. This interferometric fine structure contains the high-resolution object information.

In this paper we shall describe a detailed theory and astronomical applications of the speckle-masking method. Speckle masking has the following properties: (a) speckle masking yields true images instead of autocorrelations, (b) diffraction-limited resolution is obtained, (c) image degradation by the atmosphere and by telescope aberrations are overcome, (d) general objects can be measured, (e) no unresolvable star is required in the isoplanatic neighborhood of the object.

The features (b)–(e) are the same as for Labeyrie's speckle interferometry,[1] which stands at the beginning of all recent activities in high-resolution astrophotography. The new aspect of speckle masking is feature (a). Speckle masking goes beyond speckle holography[2-4] by way of feature (e).

Originally, speckle masking was developed for high-resolution imaging with large ground-based telescopes. However, speckle masking is also useful for high-resolution imaging with large telescopes in space. In the case of large space telescopes the speckle point spread functions are produced by permanent telescope aberrations.[21,22] The combination of speckle masking with the recently developed roll deconvolution method[21,22] or the aberration plate method[23] is useful for diffraction-limited imaging with large, aberrated space telescopes. The application of aberration plates was also investigated by Dainty.[24] The combination of speckle masking with speckle spectroscopy[25] is useful for reconstructing objective prism spectra with diffraction-limited spatial resolution. Speckle masking can also be applied to speckle interferograms of faint objects. The speckle interferograms of such objects consist of individual photon events. In this case it may be advantageous to convolve each photon-counting speckle interferogram with an Airy disk before the speckle-masking process is applied.[8]

The authors are with Physikalisches Institut der Universitat Erlangen-Nurnberg, Erwin-Rommel-Str. 1, 8520 Erlangen, Federal Republic of Germany.

Received 17 August 1983.
0003-6935/83/244028-10$01.00/0.

In Sec. II we shall introduce the concept of bispectra of speckle interferograms in order to explain the theory of speckle masking. It will be shown that a generalized transfer function of speckle masking can be defined. We have investigated this transfer function theoretically and experimentally and found that it is greater than zero for all frequencies up to the telescope cutoff frequency.

In Sec. III we shall describe two different methods for reconstructing the diffraction-limited image of the object: (1) a method which is performed in the correlation plane, (2) a recursive method which is performed in the Fourier domain. We shall show applications of both methods to astronomical data recorded with the European Southern Observatory's (ESO) 3.6-m telescope.

II. Theory of Speckle Masking based on the Concept of Bispectra of Speckle Interferograms

In this section we shall give a theoretical explanation of the astronomical speckle-masking method. The theory will be performed mainly in the Fourier domain using the concept of bispectra of speckle interferograms. In a preceding article[20] an intuitive description of speckle masking is given, which is based on triple correlations. Triple correlations and bispectra are Fourier transform pairs (see Appendix A).

In speckle masking a large number of speckle interferograms are processed to obtain a diffraction-limited image of the object. The 2-D intensity distribution $I_n(\mathbf{x})$ of the nth speckle interferogram can be described by the following incoherent, quasi-monochromatic, and space-invariant imaging equation:

$$I_n(\mathbf{x}) = O(\mathbf{x}) * P_n(\mathbf{x}) \qquad n = 1,2,\ldots,N, \tag{1}$$

where $\mathbf{x}$ denotes a 2-D vector, $O(\mathbf{x})$ is the 2-D object intensity distribution, the $*$ denotes convolution, and $P_n(\mathbf{x})$ is the combined point spread function of the telescope and the atmosphere.

For the explanation of speckle masking it may be useful to compare it with speckle interferometry[1] since most readers are probably familiar with speckle interferometry. The first step of the speckle interferometry process is the determination of the ensemble average power spectrum $\langle|\tilde{I}_n(\mathbf{u})|^2\rangle$ of many speckle interferograms $I_n(\mathbf{x})$:

$$\langle|\tilde{I}_n(\mathbf{u})|^2\rangle = |\tilde{O}(\mathbf{u})|^2 \cdot \langle|\tilde{P}_n(\mathbf{u})|^2\rangle, \tag{2}$$

where the tilde denotes Fourier transformation (see Appendix A). The brackets $\langle\ldots\rangle$ denote ensemble average over many statistically independent speckle interferograms. The function $\langle|\tilde{P}_n(\mathbf{u})|^2\rangle$ is called the speckle interferometry transfer function, which is positive and nonzero for all frequencies up to the diffraction limit. This speckle interferometry transfer function can be obtained experimentally by observing a single star, or it can be computed based on a reasonable model of the atmosphere. In any case, the speckle interferometry transfer function is smooth, practically constant over a wide range of spatial frequencies. Therefore from Eq. (2) the object power spectrum

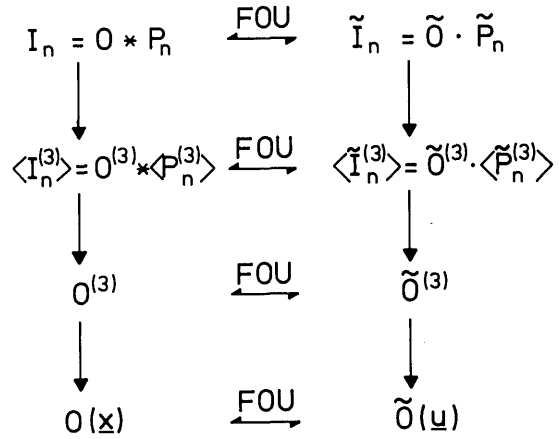

Fig. 1. Illustration of the imaging processing steps of the astronomical speckle-masking method.

$|\tilde{O}(\mathbf{u})|^2$ can be reconstructed. However, the phase of the object Fourier transform $\tilde{O}(\mathbf{u})$ is lost in speckle interferometry. Fourier transforming the object power spectrum yields the object autocorrelation. Therefore we can also say that in speckle interferometry the diffraction-limited object autocorrelation is obtained from the average autocorrelation of many speckle interferograms, i.e.,

$$\langle I_n(\mathbf{x}) \otimes I_n(\mathbf{x})\rangle \rightarrow O(\mathbf{x}) \otimes O(\mathbf{x})$$

where the $\otimes$ denotes correlation and the $\rightarrow$ denotes the compensation of the speckle interferometry transfer function.

In speckle masking the speckle interferograms are evaluated in a different way in order to preserve the phase of the object Fourier transform. In speckle masking the average triple correlation $\langle I_n^{(3)}(\mathbf{x},\mathbf{x}')\rangle$ is calculated, i.e., we evaluate the quantity

$$\begin{aligned}\langle I_n^{(3)}(\mathbf{x},\mathbf{x}')\rangle &:= \langle [I_n(\mathbf{x}) \cdot I_n)\mathbf{x} + \mathbf{x}')] \otimes I_n(\mathbf{x})\rangle \\ &= \langle \int I_n(\mathbf{x}'') \cdot I_n(\mathbf{x}'' + \mathbf{x}') \cdot I_n(\mathbf{x}'' + \mathbf{x}) d\mathbf{x}''\rangle \end{aligned} \tag{3}$$

of many speckle interferograms (see Fig. 1). The meaning of Eq. (3) is (i) the speckle interferogram $I_n(\mathbf{x})$ is multiplied with the same but shifted speckle interferograms $I_n(\mathbf{x} + \mathbf{x}')$ yielding a product mask, (ii) the product mask $I_n(\mathbf{x}) \cdot I_n(\mathbf{x} + \mathbf{x}')$ is cross correlated with $I_n(\mathbf{x})$, (iii) the ensemble average of the resulting triple correlations is calculated.

The subsequent processing steps in the speckle-masking method are such that the diffraction-limited object triple correlation $O^{(3)}(\mathbf{x},\mathbf{x}')$ is obtained from the average triple correlation $\langle I_n^{(3)}(\mathbf{x},\mathbf{x}')\rangle$ of many speckle interferograms, i.e.,

$$\langle I_n^{(3)}(\mathbf{x},\mathbf{x}')\rangle \rightarrow O^{(3)}(\mathbf{x},\mathbf{x}'),$$

where the $\rightarrow$ denotes the compensation of the speckle-masking transfer function, as shall be discussed below.

Fortunately the object triple correlation $O^{(3)}(\mathbf{x},\mathbf{x}')$ of speckle masking contains complete information about the object intensity distribution as discussed below and illustrated in Fig. 2.

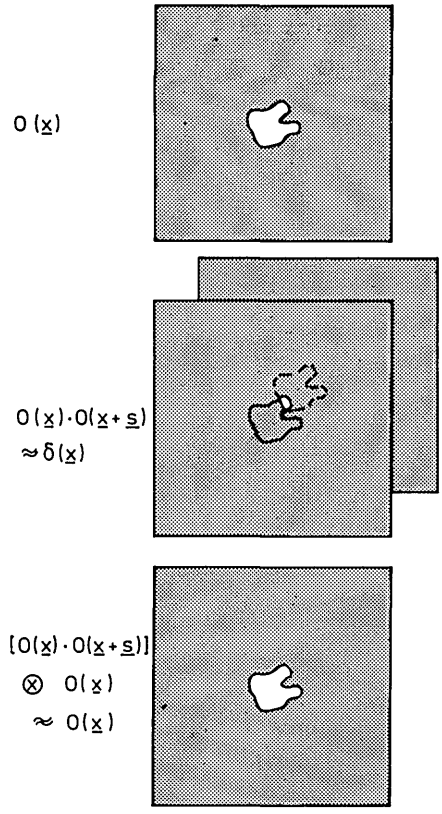

Fig. 2. Illustration of the triple correlation $O^{(3)}(\mathbf{x},\mathbf{x}'=\mathbf{s}) = [O(\mathbf{x}) \cdot O(\mathbf{x}+\mathbf{s})] \otimes O(\mathbf{x})$. If the masking vector $\mathbf{s}$ is suitably selected, a true image of the object is obtained from its triple correlation. How the object triple correlation $O^{(3)}(\mathbf{x},\mathbf{x}')$ is obtained by evaluating speckle interferograms of the object is discussed in the text.

In Fig. 2 the usefulness of the object triple correlation is illustrated by a simple example. The first step in the illustration is the multiplication of the object $O(\mathbf{x})$ with the shifted object $O(\mathbf{x}+\mathbf{s})$. The shift vector $\mathbf{x}'=\mathbf{s}$ is called the masking vector. This vector $\mathbf{s}$ is selected such that the product mask $O(\mathbf{x}) \cdot O(\mathbf{x}+\mathbf{s})$ is approximately a δ function. In this case the cross correlation of the product mask with the object yields

$$[O(\mathbf{x}) \cdot O(\mathbf{x}+\mathbf{s})] \otimes O(\mathbf{x}) \approx O(\mathbf{x}) \tag{4}$$

or equivalently $O^{(3)}(\mathbf{x},\mathbf{x}'=\mathbf{s}) \approx O(\mathbf{x})$. Therefore a true image of the object is contained in a 2-D subplane of the 4-D object triple correlation $O^{(3)}(\mathbf{x},\mathbf{x}')$. In the case of extended objects it is useful to choose a set of many different masking vectors.

For a detailed explanation it seems to be advantageous to express the processing steps by bispectra $\tilde{I}_n^{(3)}(\mathbf{u},\mathbf{v})$ rather than by triple correlations $I_n^{(3)}(\mathbf{x},\mathbf{x}')$. Both descriptions are equivalent since triple correlations and bispectra are Fourier transform pairs (see Appendix A).

In Appendix A it is shown that the bispectrum $\tilde{I}_n^{(3)}(\mathbf{u},\mathbf{v})$ can be calculated as the triple product

$$\tilde{I}_n^{(3)}(\mathbf{u},\mathbf{v}) = \tilde{I}_n(\mathbf{u})\tilde{I}_n(\mathbf{v})\tilde{I}_n(-\mathbf{u}-\mathbf{v}), \tag{5}$$

where $\tilde{I}_n(\mathbf{u})$, $\tilde{I}_n(\mathbf{v})$, and $\tilde{I}_n(-\mathbf{u}-\mathbf{v})$ are identical Fourier transforms of $I_n(\mathbf{x})$, expressed in the different variables $\mathbf{u}$, $\mathbf{v}$, and $-\mathbf{u}-\mathbf{v}$. According to Eq. (5) and Appendix A the bispectrum is separable in $\mathbf{u}$, $\mathbf{v}$, and $(-\mathbf{u}-\mathbf{v})$ functions.

In speckle masking we determine the ensemble average bispectrum $\langle \tilde{I}_n^{(3)}(\mathbf{u},\mathbf{v}) \rangle$ which is due to $I_n = O * P_n$ and due to the convolution theorem (see Appendix A) given by

$$\langle \tilde{I}_n^{(3)}(\mathbf{u},\mathbf{v}) \rangle = \tilde{O}^{(3)}(\mathbf{u},\mathbf{v}) \cdot \langle \tilde{P}_n^{(3)}(\mathbf{u},\mathbf{v}) \rangle, \tag{6}$$

where $\tilde{I}_n^{(3)}$, $\tilde{O}^{(3)}$, and $\tilde{P}_n^{(3)}$ are the bispectra of I_n, O, and P_n, respectively. Note that the bispectrum of a 2-D intensity distribution [for example, $I_n(\mathbf{x})$] is a 4-D function [for example, $|\tilde{I}_n^{(3)}(\mathbf{u},\mathbf{v})|$]. Due to this extension into the 4-D space it is possible that the phase information can survive. However, 4-D calculations can be avoided in actual application, as shown in Sec. III.

Equation (6) shows that a generalized speckle-masking transfer function $\langle \tilde{P}_n^{(3)}(\mathbf{u},\mathbf{v}) \rangle$ can be defined. We have investigated this transfer function theoretically (see Appendix B) and experimentally [see Fig. 3(a)] and found that $\langle \tilde{P}_n^{(3)} \rangle$ is real and larger than zero up to the

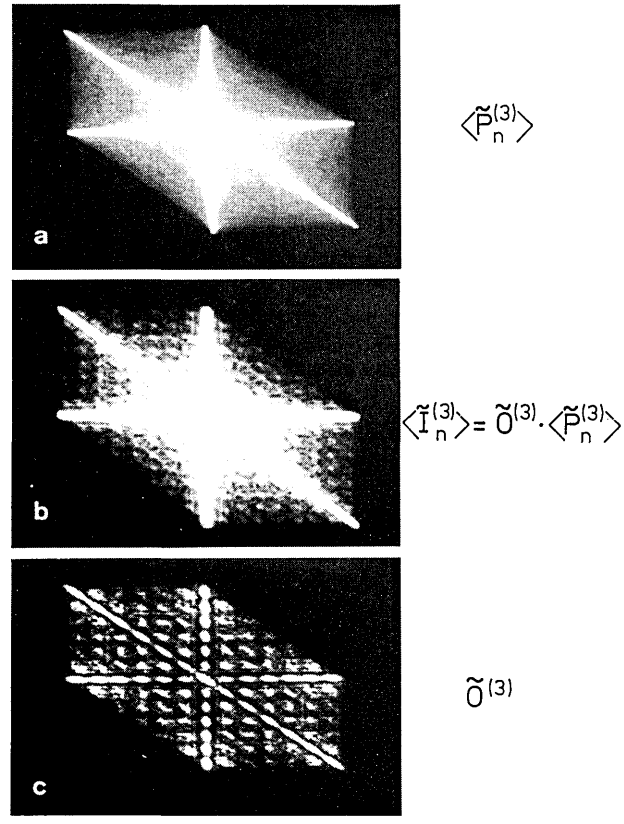

Fig. 3. Illustration of some steps in the theory of speckle masking. The raw data for these experiments were recorded with the ESO 3.6-m telescope. We produced 1-D projections of the 2-D speckle interferograms in order to avoid a 4-D transfer function $\langle \tilde{P}_n^{(3)} \rangle$. (a) Generalized speckle-masking transfer function $\langle \tilde{P}_n^{(3)}(u,v) \rangle$ calculated from 1000 speckle interferograms. (b) Average (2-D) bispectrum $\langle \tilde{I}_n^{(3)}(u,v) \rangle$ of 300 speckle interferograms of the spectroscopic double-star Omega Leonis. (c) Bispectrum $\tilde{O}^{(3)}(u,v) = \langle \tilde{I}_n^{(3)}(u,v) \rangle / \langle \tilde{P}_n^{(3)}(u,v) \rangle$ of Omega Leonis. In all three figures the moduli of the complex values are displayed.

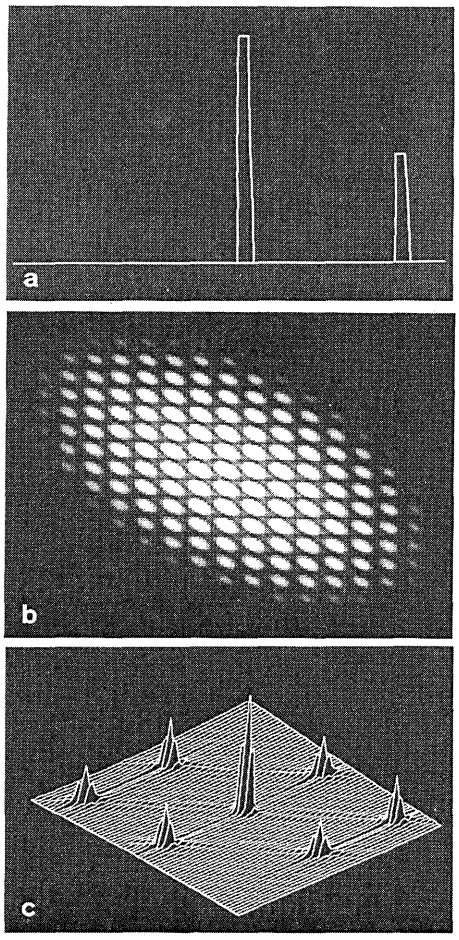

Fig. 4. Computer simulation of (a) a double star, (b) the modulus of its bispectrum, and (c) its triple correlation.

telescope cutoff frequency. Due to the reality of $\langle \tilde{P}_n^{(3)} \rangle$ the phase of the complex bispectrum of the object is identical to the phase of the average bispectrum of the object speckle interferograms, i.e.,

$$\text{phase}\,\{\langle \tilde{I}_n^{(3)}(\mathbf{u},\mathbf{v}) \rangle\} = \text{phase}\,\{\tilde{O}^{(3)}(\mathbf{u},\mathbf{v})\}. \tag{7}$$

Therefore, phase information about the object Fourier transform can be obtained directly from the average bispectrum $\langle \tilde{I}_n^{(3)} \rangle$, without compensation of any transfer function (Sec. III.B). Furthermore the transfer function $\langle \tilde{P}_n^{(3)} \rangle$ is in essence independent of telescope aberrations as shown in Appendix B.

In the remaining part of this section we will show some experimental results (Fig. 3), which illustrate Eq. (6) and especially the generalized speckle-masking transfer function $\langle \tilde{P}_n^{(3)}(\mathbf{u},\mathbf{v}) \rangle$. In this experiment we have evaluated speckle interferograms recorded with the ESO 3.6-m telescope. To avoid a 4-D transfer function, we have produced 1- D projections of the 2-D speckle interferograms. Then the generalized speckle-masking transfer function is a 2-D plane of the 4-D transfer function $\langle \tilde{P}_n^{(3)}(\mathbf{u},\mathbf{v}) \rangle$, since a projection in the correlation domain corresponds to a subplane in the Fourier inverse domain, as well known from computed tomography.[29]

Figure 3(a) shows a transfer function $\langle \tilde{P}_n^{(3)}(u,v) \rangle$ evaluated from 1000 projected speckle interferogramss of a point source. The characteristic shape of $\langle \tilde{P}_n^{(3)} \rangle$ demonstrates the inherent symmetry of bispectra (see Appendix A). Figure 3(b) shows the average bispectrum $\langle \tilde{I}_n^{(3)}(u,v) \rangle$ of 1-D projections of 300 speckle interferograms of the close spectroscopic double-star Omega Leonis. Figure 3(c) is the bispectrum of Omega Leonis calculated by $\tilde{O}^{(3)}(u,v) = \langle \tilde{I}_n^{(3)}(u,v) \rangle / \langle \tilde{P}_n^{(3)}(u,v) \rangle$, i.e., by compensating the transfer function $\langle \tilde{P}_n^{(3)}(u,v) \rangle$. For comparison, Fig. 4(b) shows the bispectrum $\tilde{O}^{(3)}(u,v)$ of a computer simulated double star [Fig. 4(a)].

III. Two Image-Reconstruction Methods

Up to now we have discussed the basic principle of speckle masking. In this section we shall describe the reconstruction of a true image $O(\mathbf{x})$ of the object from the average triple correlation $\langle I_n^{(3)}(\mathbf{x},\mathbf{x}') \rangle$ of many speckle interferograms $I_n(\mathbf{x})$. In Sec. III.A we present a method which is performed in the space domain and in Sec. III.B a method which is performed in the frequency domain.

A. Image Reconstruction in the Space Domain

To obtain the diffraction-limited image $O(\mathbf{x})$ of the object, we have to reconstruct (1) the object triple correlation $O^{(3)}(\mathbf{x},\mathbf{x}')$ from the average triple correlation $\langle I_n^{(3)}(\mathbf{x},\mathbf{x}') \rangle$ and (2) the image $O(\mathbf{x})$ from its triple correlation $O^{(3)}(\mathbf{x},\mathbf{x}')$.

Step (1) can be achieved in two different ways:

(a) Measurement of the transfer function $\langle \tilde{P}_n^{(3)}(\mathbf{u},\mathbf{v}) \rangle$ by evaluating speckle interferograms of an atronomical point source. The object bispectrum is obtained by calculating

$$\tilde{O}^{(3)}(\mathbf{u},\mathbf{v}) = \langle \tilde{I}_n^{(3)}(\mathbf{u},\mathbf{v}) \rangle / \langle \tilde{P}_n^{(3)}(\mathbf{u},\mathbf{v}) \rangle. \tag{8}$$

Finally, the object triple correlation $O^{(3)}(\mathbf{x},\mathbf{x}')$ is obtained by inverse Fourier transforming $\tilde{O}^{(3)}(\mathbf{u},\mathbf{v})$.

(b) By evaluating uncorrelated speckle interferograms of the object, as described in the text below (Gaussian speckle-masking method).

The latter method has the advantage that no astronomical point source has to be measured and that it can be performed in the correlation domain as well as in the Fourier domain. In Appendix B [Eq. (B11)] it is shown that for a Gaussian model of the atmosphere we obtain

$$\begin{aligned} I_n^{(3)}(\mathbf{x},\mathbf{x}'=\mathbf{s}) &- I_{nnm}^{(3)}(\mathbf{x},\mathbf{x}'=\mathbf{s}) - I_{nmn}(\mathbf{x},\mathbf{x}'=\mathbf{s}) \\ &- I_{nnm}^{(3)}(\mathbf{x},\mathbf{x}'=\mathbf{s}) + 2I_{nmk}^{(3)}(\mathbf{x},\mathbf{x}'=\mathbf{s}) \\ &= O^{(3)}(\mathbf{x},\mathbf{x}'=\mathbf{s}) \Rightarrow O(\mathbf{x}), \end{aligned} \tag{9}$$

where different indices in I_{nmk} indicate that uncorrelated speckle interferograms are triple correlated, as discussed in Appendices A and B.

Equation (9) can be used to calculate the triple correlation $O^{(3)}(\mathbf{x},\mathbf{x}'=\mathbf{s})$ for any masking vector $\mathbf{s}$. If $\mathbf{s}$ is selected suitably, a true image of the object is reconstructed. In the case of complicated objects it is useful to choose a set of many different masking vectors in order to improve the signal-to-noise ratio. The information about suitable masking vectors is obtained from the object autocorrelation.

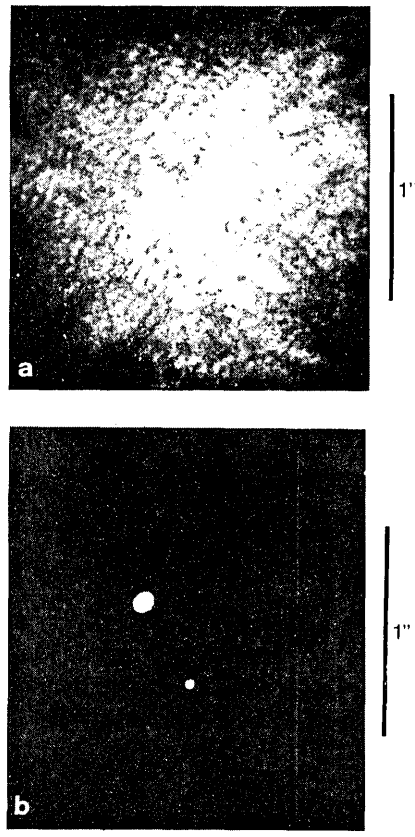

Fig. 5. Gaussian speckle-masking experiment of the close spectroscopic double-star Omega Leonis: (a) is one of the 300 evaluated speckle interferograms; (b) show the reconstruced true image of Omega Leonis. We measured (epoch: 1980.019); separation, 0.463 ± 0.004 sec of arc; position angle, 17.0 ± 1°; intensity ratio, 1.6 ± 0.3.

In Fig. 5 an application of the above described Gaussian speckle-masking method (Sec. III.A(b)] to speckle interferograms of the spectroscopic double-star Omega Leonis is shown. Figure 5(a) is one of 300 speckle interferograms which were evaluated. In Fig. 5(b) the diffraction-limited true image of Omega Leonis is shown. The raw data for the experiment were recorded with the ESO 3.6-m telescope in La Silla, Chile. In our institute we digitized the speckle interferograms with 256 × 256 pixels/frame[27] and recentered them with respect to their center of gravity. Recentering improves the compensation of the speckle-masking transfer function. We also found that high-pass filtering of the speckle interferograms is useful in order to compensate the afterglow effect of the image intensifier.

To derive Eq. (9) (see Appendix B) it was assumed that the complex light amplitude coming from an astronomical point source has Gaussian statistics in the pupil plane of the telescope. We found that the Gaussian assumption is a good approximation, although it is well known that a lognormal model is a better description of atmospheric turbulence.[28] We found experimentally that there must be a weighting constant C, which is almost 1, in front of the first term of Eq. (9), if we have nearly Gaussian statistics but not exactly. If we have exactly Gaussian statistics, C is equal to 1. To determine $C(\approx 1)$ we calculate Eq. (9) using a masking vector $\mathbf{s}'$ which is selected such that $O(\mathbf{x})$ and $O(\mathbf{x}+\mathbf{s}')$ do not overlap. For such an $\mathbf{s}'$ we obtain $[O(\mathbf{x}) \cdot O(\mathbf{x}+\mathbf{s}')] \otimes O(\mathbf{x}) = 0$ and therefore C can be determined. The processing with the wrong masking vector $\mathbf{s}'$ is a good test of whether the Gaussian assumption is fulfilled. If Gaussian statistics is not a good approximation, the processing will yield an intensity distribution consisting of two peaks, separated by the vector $\mathbf{s}'$. If there is no constant $C(\approx 1)$ such that $O^{(3)}(\mathbf{x},\mathbf{x}'=\mathbf{s}')$ becomes equal to zero or at least equal to a constant value, Eq. (9) may not be applied to compensate the speckle-masking transfer function. In this case the compensation of the speckle-masking transfer function has to be performed as described in Sec. III.A(a).

B. Recursive Image Reconstruction in the Frequency Domain

In this section we shall discuss an image-reconstruction method which unravels the complex object spectrum $\tilde{O}(\mathbf{u})$ from the object bispectrum $\tilde{O}^{(3)}(\mathbf{u},\mathbf{v})$. How $\tilde{O}^{(3)}(\mathbf{u},\mathbf{v})$ can be obtained has been discussed above. Let us assume that a sampled version $\tilde{O}^{(3)}_{p,q}$ of the object bispectrum is available,

$$\tilde{O}^{(3)}_{p,q} = \tilde{O}_p \cdot \tilde{O}_q \cdot \tilde{O}_{-p-q} \qquad p,q = -N \ldots +N, \tag{10}$$

with $\tilde{O}_P := \tilde{O}(p \cdot \Delta u)$ and $P = -N \ldots +N$, where Δu is a suitable sampling distance in the Fourier domain.

In the following the modulus and the phase of the complex object spectrum $\tilde{O}_p$ will be calculated separately. Therefore $\tilde{O}_p$ is split into

$$\tilde{O}_p = |\tilde{O}_p| \cdot \exp[i\varphi_p]. \tag{11}$$

In the recursive image-reconstruction method the modulus of the object Fourier transform is obtained as in speckle interferometry. Speckle interferometry data are produced by setting $p = 0$ (or equivalently by $q = 0$ or $p = -p$) in $\tilde{O}^{(3)}_{p,q}$, i.e.,

$$\tilde{O}^{(3)}_{0,q} = \tilde{O}_O \tilde{O}_q \tilde{O}_{-q} = \text{const} \cdot |\tilde{O}_q|^2, \tag{12}$$

where we used the fact that the spectrum of a real object is Hermitian, i.e., $O_q = O^*_{-q}$.

The next processing step is the reconstruction of the phase of the complex spectrum of the object. To this end Eq. (11) is inserted into Eq. (10). The resulting equation is split into two equations, one concerning the moduli and one concerning phase factors. The phase factors fulfill the equation

$$\exp[i\varphi_r] = \exp[i(\varphi_q + \varphi_{r-q} - \beta_{r-q,q})], \tag{13}$$

where $\beta_{r-q,q}$ is the phase of $\tilde{O}^{(3)}_{r-q,q} = |\tilde{O}^{(3)}_{r-q,q}| \exp[i\beta_{r-q,q}]$ and where the substitution $r = p + q$ was made. From Eq. (13) the phase factors $\exp[i\varphi_r]$ can be calculated recursively. It is sufficient to calculate φ_r for positive r since $\tilde{O}_r$ is Hermitian and therefore $\varphi_r = -\varphi_{-r}$. Setting $q = 1$ in Eq. (13) yields

$$\exp[i\varphi_r] = \exp[i(\varphi_1 + \varphi_{r-1} - \beta_{r-1,1})],$$
$$\varphi_0 = \varphi_1 = 0, \tag{14}$$
$$r = 2 \ldots N,$$

where the phase φ_0 is equal to zero because $\tilde{O}_p$ is Hermitian. The phase φ_1 can be set equal to zero because we are not interested in the absolute position of the reconstructed image. To explain this we start the algorithm in Eq. (14) with $r = 1$. Both φ_0 and $\beta_{0,1}$ are zero due to the reality of $O(x)$ and $O^{(3)}(x,x')$. At this point we find that φ_1 remains undeterminable, a fact that will be discussed after writing down the next iteration steps ($r = 2, r = 3 \ldots$):

$$\varphi_2 = 2\varphi_1 - \beta_{1,1},$$

$$\varphi_3 = \varphi_2 + \varphi_1 - \beta_{2,1} = 3\varphi_1 - \beta_{1,1} - \beta_{2,1},$$

$$\varphi_r = r\varphi_1 - \beta_{1,1} - \beta_{2,1} - \ldots \beta_{r-1,1}.$$

Apparently, the Fourier phase φ_r of $\tilde{O}_r$ can be determined from the phases of the bispectrum, except for the linear term $r\varphi_1$. This unknown linear phase term corresponds to the unknown position x_0 of the object $O(x - x_0)$.

The recursion given in Eq. (14) uses only the phase information contained in a single line ($q = 1$) of the object bispectrum $\tilde{O}^{(3)}_{p,q}$. Additional phase information can be obtained by setting $q = 2 \ldots N$ in Eq. (13). Therefore each phase φ_r has $(r - 1)/2$ independent representations if r is odd and $r/2$ representations if r is even. These different representations of the φ_r can be averaged. We have used Eq. (13) to find the following recursion formula which is very insensitive to noise because of the summation:

$$\exp[i\varphi_r] = \text{const} \cdot \sum_{0<q\leqq r/2} \exp[i(\varphi_q + \varphi_{r-q} - \beta_{r-q,q})], \qquad (15)$$

$$\varphi_0 = \varphi_1 = 0,$$

$$r = 2 \ldots N,$$

where the index q in the summation was selected such that all information contained in one octant of the object bispectrum is used to reconstruct the phases φ_r. The other octants of the bispectrum do not supply additional information because of the inherent symmetry of bispectra, as shown in Appendix A and illustrated in Fig. 6.

The final step in the recursive image-reconstruction method is to combine the phase factors found by Eq. (15) with the modulus of the object Fourier transform (Eq. (12)]. Inverse Fourier transformation of the complex object spectrum yields the true image of the object.

In Fig. 7 we show the result of an astronomical application of the recursive image-reconstruction method. Figure 7 is a 1-D image of the spectroscopic double-star Omega Leonis. It was reconstructed from the bispectrum of Omega Leonis shown in Fig. 3(b). Since 1-D projections of the speckle interferograms were evaluated (see Sec. II), the reconstructed image is also a projection of the object intensity distribution as discussed below. This is no limitation since a double star is a quasi-1-D object. For example, all information about the object is contained in two perpendicular projections.

In the case of general 2-D objects the recursive image-reconstruction method can be extended to two dimensions. The total algorithm consists of the following steps:

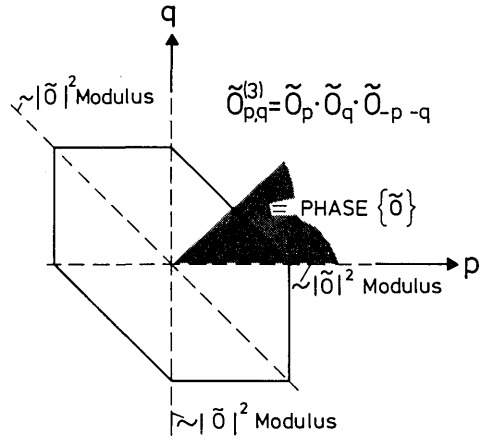

Fig. 6. Complex bispectrum $\tilde{O}^{(3)}_{p,q}$ of an object contains complete information about the modulus and the phase of the object spectrum $|\tilde{O}_r|$ (exp$[i\varphi_r]$). The modulus information $|\tilde{O}_r|$ can be reconstructed from one of the axes $p = 0$, $q = 0$, or $p = q$. The phase information (exp$[i\varphi_r[$) is contained in the area in between these distinguished axes. Because of the eightfold symmetry of the bispectrum of a real function, only one octant of the bispectrum contains nonredundant information, as indicated by the shaded area.

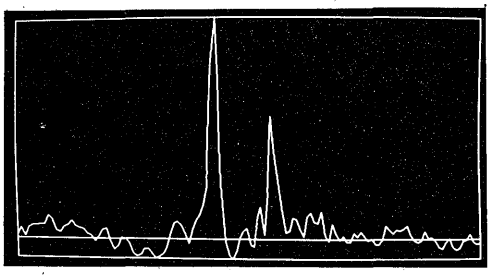

Fig. 7. Result of the recursive image reconstruction (see III.B) of the spectroscopic double-star Omega Leonis (see also Fig. 5) from its bispectrum [see Fig. 3(c)]. How the recursive image reconstruction method is extended to 2-D objects is described in the text.

(i) Collect the raw data $I_n(\mathbf{x})$.

(ii) Reconstruct the modulus of the object Fourier transform $\tilde{O}(\mathbf{u})$ as in speckle interferometry, this procedure includes the compensation of the speckle interferometry transfer function.

(iii) Reconstruct the phase of $\tilde{O}(\mathbf{u})$ from the phase of the 4-D bispectrum $\langle \tilde{I}^{(3)}_n(\mathbf{u},\mathbf{v})\rangle$, in this processing step no turbulence defects (transfer function) have to be compensated.

(iv) Combine the modulus and the phase information in order to reconstruct the object.

Only if the calculation of the 4-D bispectrum $\langle \tilde{I}^{(3)}_n(\mathbf{u},\mathbf{v})\rangle$ exceeds the storage capability of the digital equipment, we suggest the following tomography procedure. First, projections $T_n(x,\alpha_i)$ of the raw data $I_n(\mathbf{x})$ are derived. The projection angles α_i are spread out uniformly over the range 0 to π. These projections are processed as described above, yielding projections of the object. Finally an inverse projection procedure is applied in order to reconstruct the 2-D object $O(\mathbf{x})$, as known from computed tomography.[29]

IV. Summary

We have described:

(a) A detailed triple correlation or bispectrum theory of image reconstruction by speckle masking.

(b) A method for reconstructing a true diffraction-limited image from the object bispectrum.

(c) A calculation of the generalized speckle-masking transfer function. It is shown that, fortunately, the transfer function is greater than zero up to the cutoff frequency of the telescope and that the transfer function is in essence independent of telescope aberrations.

(d) Applications of the speckle-masking method to astronomical data recorded with the ESO 3.6-m telescope.

We thank the German Science Foundation (DFG) for financial support, the European Southern Observatory for observing time, and K.-D. Förster for very helpful discussions.

The work in this paper is based on data collected at the European Southern Observatory, La Silla, Chile.

Appendix A: Properties of Triple Correlations and Bispectra

In this Appendix we shall list the definitions and some properties of triple correlations and bispectra. Triple correlations and bispectra have already been used in digital and optical signal processing,[26,30–35] but a list of their properties is not available and may be useful.

The triple cross correlation of three intensity distributions $I_n(\mathbf{x})$, $I_m(\mathbf{x})$, and $I_k(\mathbf{x})$ is defined by

$$I^{(3)}_{nmk}(\mathbf{x},\mathbf{x}') = \int I_n(\mathbf{x}'')I_m(\mathbf{x}''+\mathbf{x})I_k(\mathbf{x}''+\mathbf{x}')d\mathbf{x}''. \quad \text{(A1)}$$

In this paper the $I_n(\mathbf{x})$ denote the intensity distribution of speckle interferograms and different I indices denote statistically independent speckle interferograms. If identical speckle interferograms are correlated, we use the notation $I^{(3)}_n(\mathbf{x},\mathbf{x}') = I^{(3)}_{nnn}(\mathbf{x},\mathbf{x}')$. The function $I^{(3)}_n(\mathbf{x},\mathbf{x}')$ is called triple correlation of $I_n(\mathbf{x})$.

The Fourier transform of the triple cross correlation $I^{(3)}_{nmk}(\mathbf{x},\mathbf{x}')$ is defined by

$$\tilde{I}^{(3)}_{nmk}(\mathbf{u},\mathbf{v}) = \int I^{(3)}_{nmk}(\mathbf{x},\mathbf{x}')\exp[-2\pi i(\mathbf{u}\cdot\mathbf{x}+\mathbf{v}\cdot\mathbf{x}')]d\mathbf{x}d\mathbf{x}'. \quad \text{(A2)}$$

The function $\tilde{I}^{(3)}_{nmk}(\mathbf{u},\mathbf{v})$ is also called cross bispectrum of $I_n(\mathbf{x})$, $I_m(\mathbf{x})$, and $I_k(\mathbf{x})$. Using Eqs. (A1) and (A2) yields

$$\tilde{I}^{(3)}_{nmk}(\mathbf{u},\mathbf{v}) = \tilde{I}_n(\mathbf{u})\cdot\tilde{I}_m(\mathbf{v})\tilde{I}_k(-\mathbf{u}-\mathbf{v}), \quad \text{(A3)}$$

where $\tilde{I}_n(\mathbf{u})$, $\tilde{I}_m(\mathbf{v})$, and $\tilde{I}_k(-\mathbf{u}-\mathbf{v})$ denote the Fourier transform of $I_n(\mathbf{x})$, $I_m(\mathbf{x})$, and $I_k(\mathbf{x})$, respectively.

The bispectrum of $I_n(\mathbf{x})$ is defined by

$$\tilde{I}^{(3)}_n(\mathbf{u},\mathbf{v}) = \tilde{I}^{(3)}_{nnn}(\mathbf{u},\mathbf{v}), \quad \text{(A4)}$$

especially

$$\tilde{I}^{(3)}_n(\mathbf{u},\mathbf{v}) = \tilde{I}_n(\mathbf{u})\cdot\tilde{I}_n(\mathbf{v})\cdot\tilde{I}_n(-\mathbf{u}-\mathbf{v}). \quad \text{(A4')}$$

Using Eq. (A3) several symmetry relations for bispectra can be deduced

$$\tilde{I}^{(3)}_n(\mathbf{u},\mathbf{v}) = \tilde{I}^{(3)}_n(\mathbf{v},\mathbf{u}),$$

$$\tilde{I}^{(3)}_n(\mathbf{u},\mathbf{v}) = \tilde{I}^{(3)}_n(-\mathbf{u}-\mathbf{v},\mathbf{v}), \quad \text{(A5)}$$

$$\tilde{I}^{(3)}_n(\mathbf{u},\mathbf{v}) = \tilde{I}^{(3)*}_n(-\mathbf{u},-\mathbf{v}) \quad \text{if } I_n(\mathbf{x}) \text{ is real.}$$

The last symmetry relation only holds if $I_n(\mathbf{x})$ is real and therefore $\tilde{I}_n(\mathbf{u})$ is Hermitian, that means that $\tilde{I}_n(\mathbf{u}) = \tilde{I}^*_n(-\mathbf{u})$.

Now we want to derive a convolution theorem for triple correlations. If

$$I_n(\mathbf{x}) = O(\mathbf{x}) * P_n(\mathbf{x}) = \int O(\mathbf{x}')\cdot P_n(\mathbf{x}-\mathbf{x}')d\mathbf{x}',$$

then $\tilde{I}_n(\mathbf{u}) = \tilde{O}(\mathbf{u})\cdot\tilde{P}_n(\mathbf{u})$. Combined with Eq. (A4') we obtain

$$\tilde{I}^{(3)}_n(\mathbf{u},\mathbf{v}) = \tilde{O}^{(3)}(\mathbf{u},\mathbf{v})\cdot\tilde{P}^{(3)}_n(\mathbf{u},\mathbf{v}). \quad \text{(A6)}$$

This corresponds to a convolution in the space domain

$$I^{(3)}_n(\mathbf{x},\mathbf{x}') = O^{(3)}(\mathbf{x},\mathbf{x}') ** P^{(3)}_n(\mathbf{x},\mathbf{x}'). \quad \text{(A7)}$$

Equations (A6) and (A7) refer to autobispectra and autotriple correlations. A generalization from auto to cross is straightforward.

Appendix B

1. Calculation of the Generalized Speckle-Masking Transfer Function $\langle\tilde{P}^{(3)}_n(\mathbf{u},\mathbf{v})\rangle$

In this Appendix we shall calculate the generalized transfer function of speckle masking. We use a 1-D description for the sake of simplicity without sacrificing generality.

The transfer function $\tilde{P}_n(u)$ of a space-invariant incoherent image forming system is known since Duffieux to be the autocorrelation of the pupil function $\hat{H}(\xi)$:

$$\tilde{P}_n(u) = \int \hat{H}(\xi')\hat{H}^*(\xi'+\xi)d\xi' = \int \hat{H}(\lambda fu')\hat{H}^*(\lambda fu'+\lambda fu)d(\lambda fu'). \quad \text{(B1)}$$

The variable ξ denotes the coordinate in the telescope pupil and is related to the spatial frequency by $\xi = \lambda fu$. With the scaled pupil function $H(u') = \hat{H}(\lambda fu')$ we obtain $\tilde{P}_n(u) = \int H(u')H^*(u'+u)du'$.

In astronomical imaging the light from an astronomical point source propagates through the turbulent atmosphere. Therefore the complex amplitude $H(u)$ may be split into a product of two functions, one representing the effect of the random medium $[A(u)]$ and one representing the pupil function of the telescope $[H_0(u)]$:

$$H(u) = H_0(u)\cdot A(u), \quad \text{(B2)}$$

where the function $A(u)$ can be assumed to be a stationary random variable. Substitution of Eq. (B2) into Eq. (B1) yields

$$\tilde{P}_n(u) = \int A(u')\cdot A^*(u'+u)\cdot H_0(u')\cdot H^*_0(u'+u)du', \quad \text{(B3)}$$

where $\tilde{P}_n(u)$ denotes the transfer function in the case of the nth recorded speckle interferogram.

From Eq. (B3) the transfer function of ordinary long-exposure imaging can be found by taking the ensemble average $\langle\tilde{P}_n(u)\rangle$. In the case of large telescopes $\langle\tilde{P}_n(u)\rangle$ falls off to zero for frequencies much lower than

the telescope cutoff frequency, as shown in Ref. 28, for example.

Image processing in the speckle-masking method is governed by the transfer function

$$\langle \tilde{P}_n^{(3)}(u,v)\rangle = \langle \tilde{P}_n(u)\tilde{P}_n(v)\tilde{P}_n(-u-v)\rangle. \tag{B4}$$

Substitution of Eq. (B3) into Eq. (B4) yields

$$\begin{aligned}&\langle \tilde{P}_N^{(3)}(u,v)\rangle = \\ &\iiint H_0(u')H_0^*(u'+u)H_0(v')H_0^*(v'+v)H_0(\omega)H_0^*(w-u-v)\\ &\quad\langle A(u')A^*(u'+u)A(v')A^*(v'+v)A(w)A^*(w-u-v)\rangle\\ &\quad du'dv'dw.\end{aligned} \tag{B5}$$

To calculate the sixth-order moment in Eq. (B5) we assume that the real and the imaginary parts of $A(w)$ have zero-mean Gaussian distribution. For a complex Gaussian process the momentum theorem[36] can be used to show that

$$\begin{aligned}\langle A_1A_2^*A_3A_4^*A_5A_6^*\rangle = {}&\langle A_1A_2^*\rangle\langle A_3A_4^*A_5A_6^*\rangle +\\ &\langle A_1A_2^*A_3A_4^*\rangle\langle A_5A_6^*\rangle +\\ &\langle A_1A_2^*A_5A_6^*\rangle\langle A_3A_4^*\rangle -\\ &2\langle A_1A_2^*\rangle\langle A_3A_4^*\rangle\langle A_5A_6^*\rangle +\\ &\langle A_1A_4^*\rangle\langle A_3A_6^*\rangle\langle A_5A_2^*\rangle +\\ &\langle A_1A_6^*\rangle\langle A_3A_2^*\rangle\langle A_5A_4^*\rangle,\end{aligned} \tag{B6}$$

where we have added some zeros in order to make the final result easier to discuss.

Since the complex amplitude $A(u)$ is a stationary random variable its autocorrelation function may be defined by

$$\langle A(u')\cdot A^*(u'+u)\rangle = C_A(u). \tag{B7}$$

In the following calculation we shall first discuss a special case.

Since for usual seeing conditions the complex amplitude $A(u)$ in the pupil plane has a very fine structure compared to the telescope aperture, $A(u)$ can be assumed to be δ correlated, i.e.,

$$C_A(u) = \text{const}\cdot\delta(u). \tag{B7'}$$

This approximation is not necessary for the calculation, but it makes the result easier to discuss. At the end of this section we shall discuss the general case that $A(u)$ is not δ correlated; we shall find very similar results.

Substitution of Eqs. (B7') and (B6) into Eq. (B5) yields

$$\begin{aligned}\langle \tilde{P}_n^{(3)}(u,v)\rangle = {}&\langle \tilde{P}_n(u)\rangle\langle \tilde{P}_n(v)\cdot\tilde{P}_n(-u-v)\rangle + && [1]\\ &\langle \tilde{P}_n(u)\cdot\tilde{P}_n(v)\rangle\langle \tilde{P}_n(-u-v)\rangle + && [2]\\ &\langle \tilde{P}_n(v)\rangle\langle \tilde{P}_n(u)\cdot\tilde{P}_n(-u-v)\rangle - && [3]\\ &2\langle \tilde{P}_n(u)\rangle\langle \tilde{P}_n(v)\rangle\langle \tilde{P}_n(-u-v)\rangle + && [4]\\ &\text{const}\cdot\tilde{B}^{(3)}(u,v), && [5]\end{aligned} \tag{B8}$$

where the function $\tilde{B}^{(3)}(u,v)$ is defined by

$$\begin{aligned}\tilde{B}^{(3)}(u,v) = {}&\int |H_0(w)|^2\cdot|H_0(w+u+v)|^2\\ &\times[|H_0(w+u)|^2+|H_0(w+v)|^2]^2dw.\end{aligned} \tag{B9}$$

Note that the term $\tilde{B}^{(3)}(u,v)$ in Eq. (B8) only depends on the modulus square of the pupil function of the telescope. Therefore it is independent of both, of image degradation due to atmospheric turbulence and telescope aberrations. The term $\tilde{B}^{(3)}(u,v)$ is positive and nonzero for all frequencies up to the diffraction-limit of the telescope. Terms [1], [2], [3], and [4] in Eq. (B8) contain the long-exposure transfer function $\langle \tilde{P}_n\rangle$ as a factor and therefore they are nonzero only close to the axes $u=0$, $v=0$, $u=-v$ and to the point $u=v=0$, respectively. Terms [1]–[4] cause the characteristic structure of the generalized transfer function of speckle masking, as shown in Figs. 3(a) and 8.

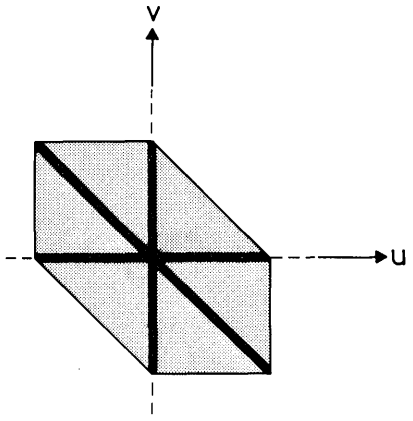

Fig. 8. Generalized speckle-masking transfer function $\langle \tilde{P}_n^{(3)}(u,v)\rangle$ is nonzero within the hexagonal area whose size is determined by the telescope cutoff frequency. The highest values are within the small hexagon surrounding the origin. This portion of the frequency domain is also accessible by long exposures. The three stripes along the two axes and along the (−45°) diagonal are medium high. The information (modulus or phase) contained in these three stripes is also obtainable by double correlations of short exposures as exploited by speckle interferometry[1] and by Knox-Thompson's algorithm.[6] The rest of the hexagon is a plateau at low level. This rest portion is the essential of the generalized speckle-masking transfer function, it permits the Fourier phase of the object to transmit. Since the phase information is obtained from a large area it has a reasonable signal-to-noise ratio.

Finally we note that the transfer function $\langle \tilde{P}_n^{(3)}(u,v)\rangle$ is a real function,. i.e., it has zero phase. This can be verified by calculating terms [1]–[4] in Eq. (B8). Using the momentum theorem, Eqs. (B3) and (B7'), one can show that terms [1]–[4] can be expressed in terms of the modulus square $|H_0(u)|^2$ of the pupil function $H_0(u)$.

In the calculation given above we assumed that the complex amplitude $A(u)$ in the pupil plane is δ correlated. If we do not make this assumption we obtain for the transfer function $\langle \tilde{P}_n^{(3)}(u,v)\rangle$ a result which differs from Eq. (B8) only in the term [5]. We find that in Eq. (B8) the function $\tilde{B}^{(3)}(u,v)$ must be substituted by a function $\tilde{B}^{(3)'}(u,v)$ which is given by

$$\begin{aligned}&\tilde{B}^{(3)'}(u,v) =\\ &\iiint H_0(u')H_0^*(u'+u)H_0(v')H_0^*(v'+v)H_0(w)H_0^*(w-u-v)\\ &[C_A(u'-v'+u)\cdot C_A(v'-w+v)\cdot C_A(-u'+w-u-v)+\\ &C_A(u'-w+u)\cdot C_A(-u'+v'+v)\cdot C_A(-v'+w-u-v)]\\ &du'dv'dw.\end{aligned}$$

2. Compensation of the Generalized Speckle-Masking Transfer Function

In this section we shall discuss how the transfer

function $\langle \tilde{P}_n^{(3)}(\mathbf{u},\mathbf{v}) \rangle$ can be compensated by evaluating uncorrelated speckle interferograms. The compensation can be performed in the correlation domain or in the Fourier domain.

Since every speckle interferogram $I_n(\mathbf{x})$ is a convolution of the object intensity distribution $O(x)$ with the nth atmospheric point spread function $P_n(x)$, Eqs. (B8) and (A6) yield

$$\begin{aligned}\tilde{O}^{(3)}(u,v) \cdot \tilde{B}^{(3)}(u,v) = {} & \langle \tilde{I}_n^{(3)}(u,v) \rangle - \\ & \langle \tilde{I}_{nmm}^{(3)}(u,v) \rangle - \langle \tilde{I}_{nnm}^{(3)}(u,v) \rangle - \\ & \langle \tilde{I}_{nmn}^{(3)}(u,v) \rangle + 2\langle \tilde{I}_{nmk}^{(3)}(u,v) \rangle \\ \approx {} & \tilde{O}^{(3)}(u,v). \end{aligned} \tag{B10}$$

The transfer function $\tilde{B}^{(3)}(u,v)$ is completely determined by the aperture shape of the telescope [see Eq. (B9)]. Therefore $\tilde{B}^{(3)}(u,v)$ is an aberration-free diffraction-limited transfer function. Certainly, $\tilde{B}^{(3)}(u,v)$ can be compensated since it is known [see Eq. (B9)] and it is greater than zero up to the telescope cutoff frequency. After this compensation the exact object bispectrum $\tilde{O}^{(3)}(u,v)$ is obtained.

Inverse Fourier transformation of Eq. (B10) yields a compensation of the generalized speckle-masking transfer function which can be performed in the correlation domain

$$\begin{aligned} O^{(3)}(x,x') ** B^{(3)}(x,x') = {} & \langle I_n^3(x,x') \rangle - \\ & \langle I_{nmm}^{(3)}(x,x') \rangle - \langle I_{nnm}(x,x') \rangle \\ & \langle I_{nmn}^{(3)}(x,x') \rangle + 2\langle I_{nmk}(x,x') \rangle \\ \approx {} & O^{(3)}(x,x'). \end{aligned} \tag{B11}$$

The function $B^{(3)}(x,x')$ is shown in Fig. 9. For an imaging system with a finite aperture of size a, the width of the function $B^{(3)}(x,x')$ is approximately $\lambda \cdot f/a$, where λ and f denote wavelength and focal length.

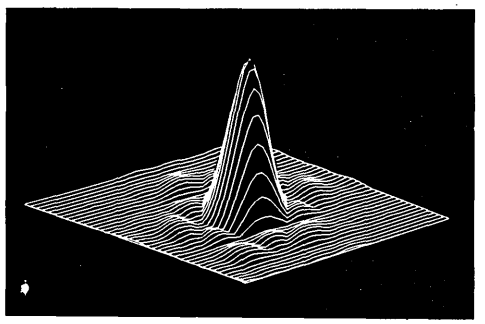

Fig. 9. Function $B^{(3)}(x,x')$ which is defined in the text.

Appendix C

1. Triple Correlations and Additive Noise

In this Appendix it is briefly discussed how triple correlations are influenced by additive noise. Let a signal $I(x)$ be contaminated by signal-independent additive noise $N(x)$, i.e.,

$$J(x) = I(x) + N(x), \tag{C1}$$

with

$$\langle N(x) \rangle = \langle N \rangle = \text{const},$$

$$\langle N(x')N(x'+x) \rangle = N^{(2)}(x).$$

The ensemble averaged triple correlation of the noisy signal $J(x)$ is

$$\begin{aligned} \langle J^{(3)}(x,x') \rangle = {} & I^{(3)}(x,x') + & [0] \\ & \langle N \rangle \cdot [I^{(2)}(x) + I^{(2)}(x') + I^{(2)}(x'-x)] + & [1] \\ & \bar{I} \cdot [N^{(2)}(x) + N^{(2)}(x') + N^{(2)}(x'-x)] + & [2] \\ & \langle N^{(3)}(x,x') \rangle, & [3] \end{aligned} \tag{C2}$$

with

$$I^{(2)}(x) = \int I(x_1) \cdot I(x_1 + x) dx_1,$$

$$\bar{I} = \int I(x) dx.$$

Therefore the ensemble averaged triple correlation of a noisy signal contains three undesired terms. Term [1] is a sum of three autocorrelation functions of the signal $I(x)$. This term becomes zero if the noise has zero mean. In a similar way term [2] contains autocorrelation functions of the noise. Term [2] vanishes for a zero-mean signal. The third term $\langle N^{(3)}(x,x') \rangle$ is a third-order moment of the noise, which usually is zero.

2. Additive Noise in the Gaussian Speckle-Masking Method

It is shown in this section that the Gaussian speckle-masking method (Sec. III.A(b)) essentially compensates the influence of additive noise in the speckle interferograms.

If noisy speckle interferograms $J_n(\mathbf{x}) = I_n(\mathbf{x}) + N_n(\mathbf{x})$ are processed in the Gaussian speckle-masking method, Eq. (9) yields

$$\begin{aligned} & \langle J_n^{(3)} \rangle - \langle J_{nmm}^{(3)} + J_{nnm}^{(3)} + J_{nmn}^{(3)} - 2J_{nmk}^{(3)} \rangle = \\ & \langle I_n^{(3)} \rangle - \langle I_{nmm}^{(3)} + I_{nnm}^{(3)} + I_{nmn}^{(3)} - 2I_{nmk}^{(3)} \rangle + & [1] \\ & \langle N_n^{(3)} \rangle - \langle N_{nmm}^{(3)} + N_{nnm}^{(3)} + N_{nmn}^{(3)} - 2N_{nmk}^{(3)} \rangle, & [2] \end{aligned} \tag{C3}$$

where we left out the variables $\mathbf{x}$ and $\mathbf{x}'$ for the sake of simplicity. To show that Gaussian speckle masking is quite insensitive to noise we must show that term [2] in Eq. (C3) is equal to zero. We shall consider three special cases:

(i) $N_n(\mathbf{x}) = \text{const} \Rightarrow \text{term [2]} = 0,$

(ii) $\langle N_n(\mathbf{x}) \rangle = 0 \Rightarrow \text{term [2]} = \langle N_n^{(3)}(\mathbf{x},\mathbf{x}') \rangle.$

Conditions (i) and (ii) mean that the Gaussian speckle-masking method is insensitive to a constant bias in the raw data and that zero-mean additive noise of skewness $[\langle N_n^{(3)}(\mathbf{x},\mathbf{x}') \rangle]$ zero is not disturbing.

Finally we consider the case of additive, nonzero-mean noise, which can be described by $N_n(\mathbf{x}) = \text{const} + N_n^0(\mathbf{x})$, where $N_n^0(\mathbf{x})$ is assumed to be zero mean. In this case we obtain

(iii) $\langle N_n(\mathbf{x}) \rangle = \text{const} \Rightarrow \text{term [2]} = \langle N_n^{(3)}(\mathbf{x},\mathbf{x}') \rangle.$

In most cases the skewness $\langle N_n^{(3)}(\mathbf{x},\mathbf{x}') \rangle$ is zero.

References

1. A. Labeyrie, Astron. Astrophys. **6**, 85 (1970).
2. C. Y. C. Liu and A. W. Lohmann, Opt. Commun. **8**, 372 (1973).

3. R. H. T. Bates, P. T. Gough, and P. J. Napier, Astron. Astrophys. **22,** 319 (1973).
4. G. P. Weigelt, Appl. Opt. **17,** 2660 (1978).
5. C. R. Lynds, S. P. Worden, and J. W. Harvey, Astrophys. J. **207,** 174 (1976).
6. K. T. Knox and B. J. Thompson, Astrophys. J. Lett. **193,** L45 (1974).
7. D. C. Ehn and P. Nisenson, J. Opt. Soc. Am. **65,** 1196 (1975).
8. G. P. Weigelt, Opt. Commun. **21,** 55 (1977).
9. R. H. T. Bates, M. O. Milner, G. I. Lund, and A. D. Seager, Opt. Commun. **26,** 22 (1978).
10. K. von der Heide, Astron. Astrophys. **70,** 777 (1978).
11. J. R. Fienup, Opt. Lett. **3,** 27 (1978).
12. B. J. Brames and J. C. Dainty, J. Opt. Soc. Am. **71,** 1542 (1981).
13. J. G. Walker, Appl. Opt. **21,** 3132 (1982).
14. L. N. Mertz, Appl. Opt. **18,** 611 (1979).
15. W. J. Cocke, Proc. Soc. Photo-Opt. Instrum. Eng. **231,** 11 (1980).
16. C. Roddier, F. Roddier, and J. Vernin, in *Proceedings, ESO Conference on Scientific Importance of High Angular Resolution at IR and Optical Wavelengths*, M. H. Ulrich and K. Kjär, Eds. (ESO, Garching, Germany, 1981), p. 165.
17. A. M. J. Huiser, Opt. Commun. **42,** 226 (1982).
18. A. H. Greenaway, Opt. Commun. **42,** 157 (1982).
19. R. H. T. Bates and F. M. Cady, Opt. Commun. **32,** 365 (1980).
20. G. P. Weigelt and B. Wirnitzer, Opt. Lett. **8,** 389 (1983).
21. A. W. Lohmann and G. Weigelt, in *Proceedings, ESA/ESO Workshop on Astronomical Uses of the Space Telescope*, F. Macchetto, F. Pacini, and M. Tarenghi, Eds. (ESO, Geneva, 1979), p. 353.
22. G. Weigelt, Proc. Soc. Photo-Opt. Instrum. Eng. **332,** 284 (1982).
23. G. Weigelt, in *Proceedings, Conference on Image Processing in Astronomy*, G. Sedmak, M. Capaccioli, and R. J. Allen, Eds. (Osservatorio Astronomico di Trieste, Trieste, Italy, 1979), p. 422.
24. J. C. Dainty, Opt. Commun. **7,** 129 (1973).
25. G. Weigelt, in *Proceedings, ESO Conference on Scientific Importance of High Angular Resolution at IR and Optical Wavelengths*, M. H. Ulrich and K. Kjar, Eds. (ESO, Garching, Germany, 1981), p. 95.
26. T. R. Bader, Proc. Soc. Photo-Opt. Instrum. Eng. **185,** 140 (1979).
27. G. Baier and G. Weigelt, Astron. Astrophys. **121,** 137 (1983).
28. J. C. Dainty, in *Laser Speckle and Related Phenomena*, J. C. Dainty, Ed. (Springer, Berlin, 1975).
29. H. H. Barrett and W. Swindell, *Radiological Imaging: Theory and Image Formation, Detection and Processing* (Academic, New York, 1981), Vols. 1 and 2.
30. K. Sasaki, T. Sato, and Y. Namamura, IEEE Trans. Sonics Ultrasón. **SU-24,** 193 (1977).
31. H. Gamo, J. Appl. Phys. **34,** 875 (1963).
32. D. Casasent and G. Silbershatz, Appl. Opt. **21,** 2076 (1982).
33. J. Cohen, Proc. Soc. Photo-Opt. Instrum. Eng. **180,** 134 (1979).
34. P. Kellman, Opt. Eng. **19,** 370 (1980).
35. J. W. Goodman, Aust. J. Electr. Electron. Eng. **2,** 140 (1982).
36. I. S. Reed, IRE Trans. Inf. Theory **IT-8,** 194 (1964).

Patter *continued from page 3987*

concentration of an impurity when there is no redistribution of impurities. For example, the rule is set for iron (A). The impurity concentration in atomic parts per million (ppma) is read for the allowable degradation in cell efficiency. For a 10% degradation, the allowable iron concentration is 7×10^{-3} ppma (B).

Scales 3, 4, and 5 are used when a redistribution of impurities occurs. First, the impurity-buildup (IB) factor is determined. For five sequential replenishments (C), the IB factor is 46 if 90% of the melt is grown between replenishments (D). If iron is set at this IB factor (E), the tolerable iron concentration in the silicon feedstock is then 23 ppma for a 10% degradation in cell performance (E).

This work was done by Kazuo A. Yamakawa of Caltech for Nasa's Jet Propulsion Laboratory. Refer to NPO-15646.

Ultrasonics and optics control shot size

A proposed feedback system would assure the production of silicon shot of uniform size. The new control method is particularly advantageous in that constant size could be maintained even while other process variables are changed deliberately or inadvertently (for example, the increase in nozzle diameter with erosion).

As shown in Fig. 17, a piezoelectric ultrasonic transducer is placed on the nozzle to vibrate the silicon stream. The shot size is determined, in part, by the wavelength of vibrations in the liquid stream as it breaks up into drops. Thus, the vibration frequency can be varied to control the shot size. The drops fall through a light beam/photodetector apparatus that measures their size. The photodetector output is used to control the vibrator frequency and thus to maintain shot size at the desired value.

While the new control system was proposed for silicon-shot production, it is applicable to other materials as well. Some experimentation will be necessary to determine nozzle diameters, drop sizes, vibration frequencies, and other process variables for each material.

This work was done by Andrew D. Morrison of Caltech for NASA's Jet Propulsion Laboratory. Refer to NPO-15608.

Annealing solar cells with lasers

A laser can anneal silicon solar cells rapidly enough for use in production, according to a recent study. The laser is a frequency-doubled Nd:YAG device. The 30-m diameter spot formed by the laser covers enough area to process silicon wafers rapidly.

The laser is intended for use on solar cells in which pn junctions have been formed by ion implantation—a technique that is likely to replace the standard thermal-diffusion method of forming junctions in cells because of the high automation potential. However, a major problem with ion implantation is that a thin layer at the surface of the silicon is damaged, often losing its crystal structure and becoming completely amorphous.

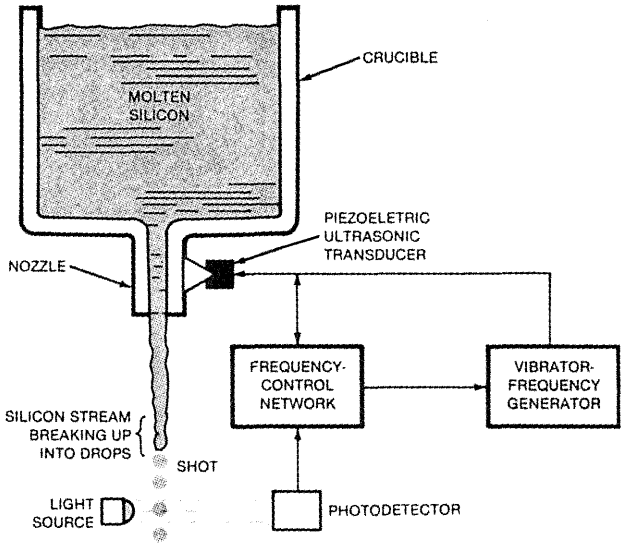

Fig. 17. Breakup of a silicon stream into drops is controlled, in part, by varying the frequency of vibrations imparted to the stream by an ultrasonic transducer. Drop size is monitored by the photodetector.

continued on page 4047